

DYSINK: DYNAMIC FRAME SINKS FOR AUTOREGRESSIVE LONG VIDEO GENERATION

Bo Ye^{1,2,3}, Xinyu Cui⁵, Jian Zhao^{3,4}, Tong Wei^{1,2}, Min-Ling Zhang^{1,2}

¹School of Computer Science and Engineering, Southeast University

²Key Lab. of Computer Network and Information Integration, Southeast University

³Zhongguancun Academy

⁴Zhongguancun Institute of Artificial Intelligence

⁵Institute of Automation, CAS

ABSTRACT

Autoregressive long video generation often adopts bounded-memory streaming for efficiency, typically combining local windows for short-term continuity with static early-frame sinks as long-range anchors. However, this fixed allocation keeps early frames cached even when the current visual state has substantially diverged from them, while discarding potentially more relevant intermediate history. As a result, the retained long-range context may become less adaptive and bias generation toward outdated cues; in severe cases, RoPE-induced phase re-alignment can homogenize inter-head attention and cause sink collapse, where content regresses toward sink frames. We propose *DySink*, a retrieval-based framework that maintains a compact memory bank and selects visually relevant historical frames as dynamic frame sinks. *DySink* couples adaptive retrieval with a sink anomaly gate, which detects excessive inter-head consensus over retrieved context and suppresses collapse-prone context. Experiments on minute-long videos show that *DySink* consistently improves dynamic degree over strong baselines while also achieving higher temporal quality. The code and model weights will be released at <https://github.com/yebo0216best/DySink>.

1 INTRODUCTION

Diffusion-based video generation has advanced rapidly, with systems such as Sora (OpenAI, 2024), Wan (Wan et al., 2025), and Seedance (Seedance et al., 2026) demonstrating impressive visual fidelity and motion realism. Despite this progress, extending generation from short videos (e.g., 5–10 seconds) to long-horizon videos remains challenging. A major bottleneck lies in the quadratic cost of bidirectional diffusion transformers (Peebles & Xie, 2023) over spatiotemporal tokens, which makes direct long-horizon video generation computationally prohibitive. To improve scalability, recent studies have turned to autoregressive streaming paradigms, where videos are generated sequentially with causal attention and KV caching. This formulation enables scalable long-horizon generation with bounded memory. Representative methods, including CausVid (Yin et al., 2025), Self-Forcing (Huang et al., 2025), Self-Forcing++ (Cui et al., 2025), Rolling-Forcing (Liu et al., 2025), and LongLive (Yang et al., 2025), progressively extend generation horizons to minutes by combining streaming training with bounded historical context. Under this setting, a central design question is how to allocate the limited historical cache so that the model can maintain temporal continuity and long-range consistency. Recent methods (Liu et al., 2025; Yang et al., 2025) commonly address this issue by combining sliding-window attention with *frame-level attention sinks* (hereafter, *frame sinks*) (Xiao et al., 2023). In this design, a local window retains recent frames for short-term continuity, while several early frames are cached as global anchors for long-term consistency.

Despite their empirical success, static frame sinks impose a fixed memory allocation that may become suboptimal in long rollouts. Under a bounded memory budget, sliding-window attention may discard intermediate frames that better match later visual states, while early sink frames remain persistently cached even after the visual state has substantially evolved. As a result, the model may rely on outdated anchors rather than more relevant historical frames, biasing generation toward misaligned

visual cues (Yang et al., 2026b). This suggests that the issue lies not in long-range conditioning itself, but in the static selection of long-range context: early-frame anchors can provide useful stabilizing cues, yet their fixed allocation becomes less adaptive as generation evolves. In more severe cases, Cui et al. (2026) identify sink collapse, where generated content repeatedly regresses toward sink frames, producing abrupt scene resets and cyclic motion patterns. Their analysis attributes this collapse to phase re-alignment under RoPE (Su et al., 2024) and inter-head attention homogenization, where many attention heads simultaneously assign high weights to sink frames.

In this work, we propose DySink for adaptive long-range memory selection in autoregressive long video generation. Rather than keeping the earliest frames as persistent anchors, DySink maintains a compact memory bank and retrieves historical frames that are visually relevant to the current generation context. These retrieved frames serve as dynamic frame sinks, providing long-range conditioning without persistent reliance on fixed early-frame anchors. To reduce sink-collapse-prone attention patterns, DySink couples retrieval with a lightweight per-layer sink anomaly gate. The gate is motivated by the observation that sink collapse is associated not with a single attention head, but with excessive inter-head consensus, where many heads simultaneously over-attend to sink-like historical context. Instead of modifying RoPE with multi-head RoPE jitter (Cui et al., 2026), DySink preserves the original positional encoding structure and treats abnormal consensus over retrieved context as a signal that the selected memory may be collapse-prone. When such consensus is detected, the gate suppresses the corresponding retrieved KV context for that layer and falls back to the sliding-window context. This design combines adaptive memory selection with layer-wise context control, reducing outdated conditioning while suppressing collapse-prone retrieved context.

Our contributions are summarized as follows:

- We propose a dynamic frame-sink retrieval mechanism that selects visually relevant historical frames as long-range anchors, reducing reliance on fixed early-frame sinks.
- We design a lightweight per-layer sink anomaly gate that detects excessive inter-head consensus over retrieved context and suppresses collapse-prone context without modifying the RoPE formulation.
- Experiments on minute-long video generation show that DySink improves Dynamic Degree by 6.60–8.16 points over strong baselines while also achieving higher measured Temporal Quality, demonstrating the benefit of dynamic frame sinks for long-horizon generation.

2 RELATED WORK

2.1 AUTOREGRESSIVE VIDEO DIFFUSION

Autoregressive video diffusion has emerged as a practical paradigm for streaming video generation, where future frames or chunks are generated causally from previously synthesized content. CausVid (Yin et al., 2025) distills bidirectional video diffusion models into few-step causal generators with KV caching, while Self-Forcing (Huang et al., 2025) reduces the train–test gap by rolling out the model on its own predictions during training. Subsequent works further improve this paradigm through stronger rollout training, distillation, or optimization objectives: Self-Forcing++ (Cui et al., 2025) and Rolling-Forcing (Liu et al., 2025) improve long-horizon stability, Reward Forcing (Lu et al., 2025) enhances motion dynamics with reward-weighted distribution matching, and Resampling Forcing (Guo et al., 2025) studies teacher-free training with self-resampled histories. Helios (Yuan et al., 2026) further explores real-time long-video generation at larger model scale. These methods mainly address how to obtain robust and efficient autoregressive generators. Causal Forcing (Zhu et al., 2026) further improves autoregressive distillation by using an autoregressive teacher for causal ODE initialization, addressing the architectural gap between bidirectional teachers and causal students. In this work, our focus is complementary: given such a generator, DySink studies how its historical context should be selected and reused during long rollouts.

2.2 LONG VIDEO GENERATION

Long video generation requires maintaining scene identity and temporal coherence across extended rollouts while allowing the visual content to evolve over time. A common solution is to restrict attention to a sliding window, which enables scalable generation but discards distant context. To compensate, frame sinks have been adopted as persistent global anchors. LongLive (Yang et al., 2025)

and Rolling Forcing (Liu et al., 2025) retain early frames as static frame sinks. LoL (Cui et al., 2026) further identifies a sink-collapse failure mode in ultra-long autoregressive generation, where generated content repeatedly regresses toward sink frames. Related methods improve long-range memory by enlarging, updating, compressing, or structuring historical context: Deep Forcing (Yi et al., 2025) uses deep sinks with training-free KV compression, Reward Forcing (Lu et al., 2025) updates sink states with EMA, Relax Forcing (Zhao et al., 2026) decomposes history into Sink, Tail, and History regions, VideoSSM (Yu et al., 2025b) maintains a SSM-based compressed global memory, and Pretraining Frame Preservation (Zhang et al., 2025) learns lightweight history embeddings. For interactive or narrative generation, Anchor Forcing (Yang et al., 2026a) designs anchor-guided re-caching for prompt switches. Context-as-Memory (Yu et al., 2025a) treats historical frames as memory and retrieves relevant context according to camera-trajectory-based FOV overlap, enabling scene-consistent interactive long-video generation. MemFlow (Ji et al., 2025) retrieves prompt-relevant historical cues. Unlike these methods that rely on static, compressed, rule-updated, camera-guided, or prompt-relevant memories, DySink retrieves visually relevant historical KV states from a dynamic memory bank and further controls collapse-prone retrieved context with the sink anomaly gate.

3 PRELIMINARY

3.1 VIDEO DIFFUSION MODELS

We briefly review the flow-matching formulation (Lipman et al., 2022; Esser et al., 2024) used by modern diffusion transformers (DiTs) (Peebles & Xie, 2023), including Wan2.1 (Wan et al., 2025). Let $\mathbf{x}_0 \sim q(\mathbf{x}_0)$ denote a clean video latent sampled from the data latent distribution q , where the subscript 0 indicates the data endpoint of the diffusion trajectory. Let $\epsilon \sim \mathcal{N}(\mathbf{0}, \mathbf{I})$ denote a standard Gaussian noise latent with the same shape as \mathbf{x}_0 , where $\mathbf{0}$ and \mathbf{I} are the zero mean and identity covariance, respectively. Following the convention where $t=0$ corresponds to data and $t=1$ to noise, the forward process linearly interpolates between \mathbf{x}_0 and ϵ :

$$\mathbf{x}_t = (1 - t)\mathbf{x}_0 + t\epsilon, \quad t \in [0, 1], \quad (1)$$

where \mathbf{x}_t denotes the latent state at diffusion time t . The corresponding velocity field is $\frac{d\mathbf{x}_t}{dt} = \epsilon - \mathbf{x}_0$. A velocity network \mathbf{v}_θ , parameterized by θ , is trained by minimizing:

$$\mathcal{L}_{\text{FM}} = \mathbb{E}_{\mathbf{x}_0 \sim q, \epsilon \sim \mathcal{N}(\mathbf{0}, \mathbf{I}), t \sim \mathcal{U}[0, 1]} \left[\left\| \mathbf{v}_\theta(\mathbf{x}_t, t) - (\epsilon - \mathbf{x}_0) \right\|_2^2 \right], \quad (2)$$

where \mathcal{L}_{FM} is the flow-matching objective, $\mathcal{U}[0, 1]$ is the uniform distribution over diffusion time, and $\|\cdot\|_2$ denotes the Euclidean norm. We omit text conditioning in this subsection for notational simplicity. At inference, an ordinary differential equation (ODE) solver integrates the learned velocity field from $t=1$ to $t=0$ to generate a clean video latent. Wan2.1 employs a causal 3D VAE to compress a raw video clip $\mathbf{V} \in \mathbb{R}^{T \times H \times W \times 3}$ into a latent $\mathbf{x}_0 \in \mathbb{R}^{T' \times H' \times W' \times C}$, where T, H, W denote the number of frames, height, and width of the input video, T', H', W' denote the corresponding latent dimensions, and C is the latent channel dimension. The spatial and temporal downsampling factors are approximately $8\times$ and $4\times$, respectively. Its causal temporal convolutions avoid dependence on future frames, enabling sequential video processing without future information leakage.

3.2 AUTOREGRESSIVE VIDEO GENERATION

Generating long videos with standard DiTs is computationally prohibitive, as bidirectional self-attention scales quadratically with the number of spatiotemporal tokens. To enable long-horizon generation, we adopt an autoregressive DiT formulation that generates frames sequentially under causal conditioning (Yin et al., 2025). Let n denote the step index, and let $\mathbf{x}^{(n)}$ denote the latent frames generated at step n , where each step produces L latent frames. At each step, generation is conditioned on a text prompt embedding \mathbf{c} and a bounded historical key-value (KV) cache $\mathcal{K}_{<n}$, which stores selected KV states from frames generated before step n . Concretely, starting from a Gaussian noise latent $\mathbf{x}_1^{(n)} \sim \mathcal{N}(\mathbf{0}, \mathbf{I})$, the model solves the following conditional generation ODE:

$$\frac{d\mathbf{x}_t^{(n)}}{dt} = \mathbf{v}_\theta(\mathbf{x}_t^{(n)}, t, \mathbf{c}, \mathcal{K}_{<n}), \quad t: 1 \rightarrow 0, \quad (3)$$

where $\mathbf{x}_t^{(n)}$ is the noisy latent state of the n -th generated segment at diffusion time t . The clean latent output of this autoregressive step is obtained as:

$$\hat{\mathbf{x}}_0^{(n)} = \text{ODESolve}_{t:1 \rightarrow 0} \left(\mathbf{x}_1^{(n)}; \mathbf{v}_\theta(\cdot, t, \mathbf{c}, \mathcal{K}_{<n}) \right), \quad (4)$$

where $\hat{\mathbf{x}}_0^{(n)}$ denotes the generated clean latent segment at step n . To keep memory consumption bounded, prior methods typically restrict $\mathcal{K}_{<n}$ to two types of historical context: **(i)** static frame sinks, which retain the KV caches of early frames as global anchors for long-term consistency; and **(ii)** sliding-window attention, which keeps the W most recently generated frames for short-term continuity. Let S denote the number of static sink frames and W denote the local-window size. Together, these components bound the cache size by at most $S + W$ frames, supporting long-horizon rollout with KV-memory overhead that remains constant with respect to the rollout length.

4 METHOD

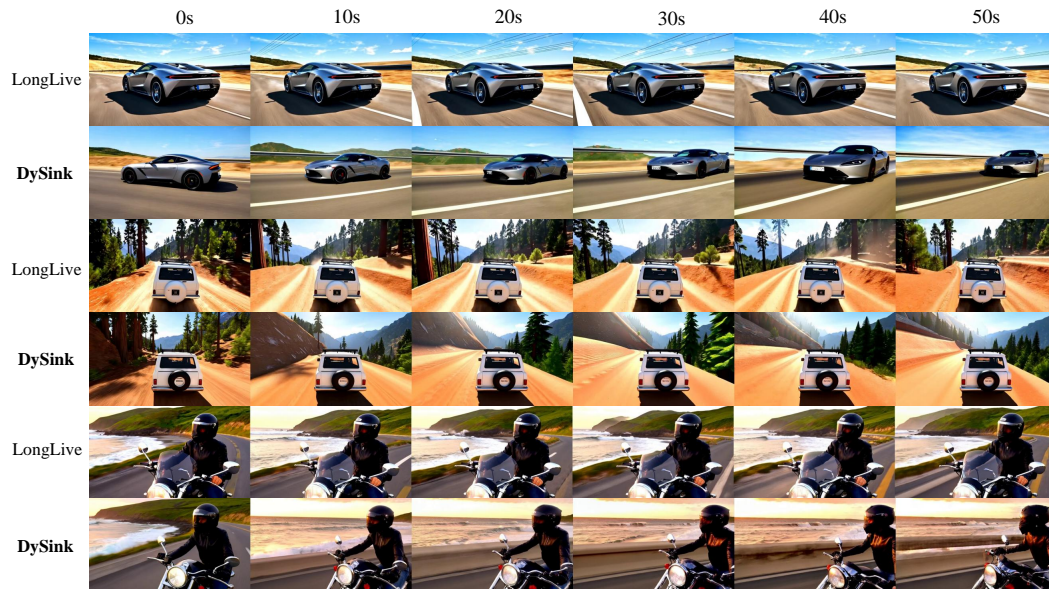


Figure 1: **Qualitative motivation.** We compare the static-sink baseline LongLive (Yang et al., 2025) with DySink over 50s rollouts. Static frame sinks reuse early frames as long-range anchors, which may bias later generation toward outdated visual states. DySink retrieves visually relevant historical frames as dynamic anchors, preserving coherence while allowing adaptive evolution.

4.1 MOTIVATION

Autoregressive long video generation requires long-range semantic and visual consistency across extended frame sequences, exceeding the effective receptive field of sliding-window attention. Recent methods (Yang et al., 2025; Liu et al., 2025) address this limitation using frame sinks, where early frames are permanently cached as global anchors. However, as generation progresses, the current visual state may substantially diverge from these early-frame anchors. Retaining such outdated anchors creates a conditioning mismatch that biases the model toward reproducing sink-frame attributes (Yang et al., 2026b). Consequently, excessive reliance on static sinks can reduce adaptability to scene evolution and motion changes, and in severe cases may lead to sink-collapse-like failures such as abrupt scene resets or cyclic motion patterns. Figure 1 qualitatively illustrates this limitation: the static-sink baseline preserves appearance consistency, but shows limited visual evolution and repeatedly revisits early visual configurations over long rollouts.

A natural alternative is to select historical context adaptively, rather than treating the earliest frames as permanent anchors. When the retrieved history is visually aligned with the current generation window,

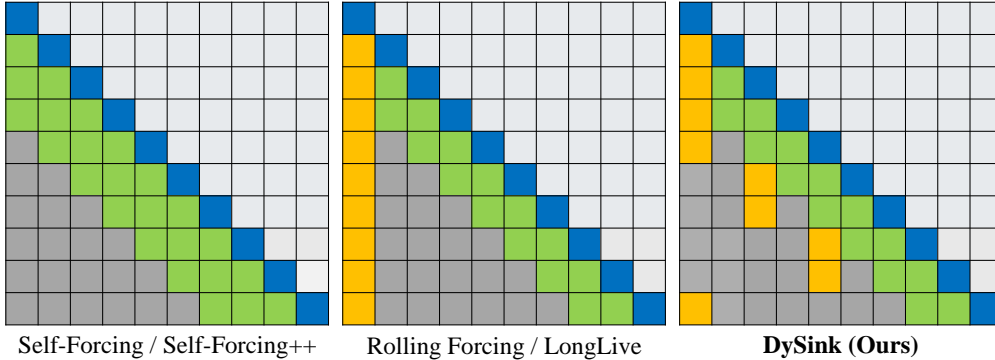


Figure 2: **Comparison of attention patterns for autoregressive long video generation.** Blue, green, yellow, and gray cells denote current frames, local-window frames, long-range anchor frames, and inactive historical frames, respectively. Self-Forcing (Huang et al., 2025) and Self-Forcing++ (Cui et al., 2025) use only local-window frames, causing distant history to be discarded. Rolling Forcing (Liu et al., 2025) and LongLive (Yang et al., 2025) introduce static frame sinks for long-range consistency. DySink retrieves relevant historical frames as frame sinks.

it can provide non-local structural cues while reducing the risk of imposing outdated visual priors. Motivated by this, we propose DySink, a retrieval-based alternative to static frame sinks. DySink maintains a dynamic memory bank of historical frames, indexed by compact visual descriptors, and retrieves visually relevant key-value states according to the current local context. This content-adaptive memory mechanism retains long-range conditioning without permanently relying on early frames, with the goal of reducing conditioning mismatch.

When generation extends to long horizons, static frame sinks may suffer from sink collapse, where generated content regresses toward sink frames, resulting in cyclic motion patterns and sudden scene resets. Prior analysis attributes this phenomenon to the periodic structure of RoPE: long-range phase re-alignment causes multiple attention heads to simultaneously over-attend to sink frames, leading to inter-head attention homogenization (Cui et al., 2026). Notably, a small subset of heads with high sink attention does not cause collapse; instead, the collapse emerges when a large fraction of heads simultaneously exhibit anomalously high attention to sink frames. While LoL (Cui et al., 2026) mitigates this by applying multi-head RoPE jitter to shift the base frequencies of different attention heads, DySink instead adopts a memory-control strategy. Our sink anomaly gate treats excessive inter-head consensus on retrieved historical frames as an indicator of collapse-prone context, and suppresses the corresponding retrieved KV states without modifying the RoPE frequency structure.

4.2 THE DYSINK FRAMEWORK

DySink decomposes long-range memory control into two decisions: which historical context should be reused, and when the selected context should be trusted. The retrieval addresses the first decision by selecting relevant historical context, while the sink anomaly gate addresses the second by suppressing retrieved context that induces excessive inter-head consensus. For implementation efficiency, DySink stores and retrieves these historical frames in temporal blocks; each memory entry corresponds to a block containing multiple latent frames.

Memory bank construction. DySink maintains a memory bank \mathcal{M} over previously generated video blocks, where each entry is defined as $(\mathbf{f}_i, \mathcal{K}_i)$. Here $\mathbf{f}_i \in \mathbb{R}^d$ is a compact visual descriptor of block i , and $\mathcal{K}_i = \{(\mathbf{K}_i^{(\ell)}, \mathbf{V}_i^{(\ell)})\}_{\ell=1}^{N_{\text{layer}}}$ denotes the layer-wise key-value caches. To construct \mathbf{f}_i , the latent frames of block i are first decoded into pixel space and then encoded by a frozen visual encoder. The resulting frame-wise features are subsequently aggregated via mean pooling and ℓ_2 normalization (Bolya et al., 2025):

$$\mathbf{f}_i = \text{Norm} \left(\frac{1}{N_i} \sum_{r=1}^{N_i} \text{VisualEncoder}(v_i^{(r)}) \right), \quad (5)$$

where N_i is the total number of pixel frames in block i . This block-level representation captures short-term temporal structure while yielding discriminative features for retrieval. We adopt a visual-only indexing scheme, as visual similarity provides the dominant signal for temporal coherence.

To maintain a compact and high-quality memory bank, we use a novelty-aware update strategy. The first blocks are inserted to initialize the memory bank, but are not privileged during retrieval. Thereafter, a candidate block is admitted only if it is sufficiently dissimilar to existing entries: $\max_{m \in \mathcal{M}} \cos(\mathbf{f}_i, \mathbf{f}_m) \leq \tau_{\text{dedup}}$. This criterion suppresses redundant storage and prevents the memory bank from being dominated by highly similar content. Moreover, when near-duplicate blocks arise, earlier entries are preferentially maintained, as they are generally less corrupted by long-term error accumulation and thus provide more reliable anchors. Finally, memory entries not used by the current step are offloaded to CPU memory, so the GPU-resident historical context remains bounded by the local window and the retrieved entries.

Memory retrieval and injection. Let W_j denote the set of block indices within the local sliding window immediately preceding block j . For each block $w \in W_j$, we compute its descriptor f_w using the same procedure as in Eq. 5. Given a target block j , DySink retrieves relevant historical context from the memory bank \mathcal{M} in a content-adaptive manner. During retrieval, we exclude memory entries that already fall inside the current sliding window to avoid duplicating local context after KV concatenation. We aggregate blocks within sliding window \mathcal{W}_j as retrieval queries and compute the relevance score of a memory entry i as

$$s(i, j) = \frac{1}{|\mathcal{W}_j|} \sum_{w \in \mathcal{W}_j} \cos(\mathbf{f}_w, \mathbf{f}_i), \quad (6)$$

where $\cos(\cdot, \cdot)$ denotes cosine similarity. This formulation conditions retrieval on the recent generation context while smoothing transient frame-level variations. We then select the top- k eligible memory entries with the highest relevance scores. The corresponding KV caches of the selected entries are transferred to GPU memory. For each DiT layer ℓ , the retrieved KV caches and the local sliding-window KV caches are concatenated to form the attention context:

$$\mathbf{K}_{\text{attn}}^{(j, \ell)} = \text{Concat}_{\text{token}}\left(\mathbf{K}_{\text{ret}}^{(j, \ell)}, \mathbf{K}_{\text{loc}}^{(j, \ell)}\right), \quad \mathbf{V}_{\text{attn}}^{(j, \ell)} = \text{Concat}_{\text{token}}\left(\mathbf{V}_{\text{ret}}^{(j, \ell)}, \mathbf{V}_{\text{loc}}^{(j, \ell)}\right). \quad (7)$$

Unlike prior approaches that rely on static frame sinks, DySink dynamically retrieves visually relevant historical context from the memory bank, thereby reducing conditioning mismatch and alleviating the structural bias toward early frames.

Sink anomaly gate. Dynamic frame sinks provide visually relevant historical context, but long-horizon generation can still be affected by sink-collapse attention patterns. Prior analysis shows that, under RoPE, sink-collapse is associated with phase re-alignment to sink frames and inter-head attention homogenization: the failure is not attributed to a single attention head, but occurs when many heads simultaneously assign high attention weights to sink frames, resulting in a degeneracy of attention diversity (Cui et al., 2026). Existing methods mitigate this issue via multi-head RoPE jitter, which shifts the base frequencies of different attention heads to break such inter-head homogenization. In contrast, we introduce a lightweight per-layer anomaly gate that uses excessive inter-head consensus as a practical indicator of collapse-prone retrieved context. When the retrieved historical frames attract an abnormally large fraction of attention heads compared with the local context, the gate suppresses the retrieved KV states in the layer-wise attention context and falls back to the local-window frames, without modifying the RoPE frequency structure.

Formally, let $\mathbf{Q}^{(j, \ell)} \in \mathbb{R}^{T_q \times H \times d_h}$ denote the queries at layer ℓ for the current block j , where T_q is the number of query tokens in this block. Let $\mathbf{K}_{\text{loc}}^{(j, \ell)}$ denote the corresponding local-window keys. Suppose we retrieve the top- k most relevant memory blocks from the bank, denoted as $\{\mathbf{K}_{\text{ret}, e}^{(j, \ell)}\}_{e=1}^k$. To quantify excessive inter-head consensus, we first compute a head-wise representative query $\bar{\mathbf{q}}_h^{(j, \ell)} = \frac{1}{T_q} \sum_{t=1}^{T_q} \mathbf{Q}_{t, h}^{(j, \ell)}$. For a key set \mathbf{K} , let $|\mathbf{K}|$ denote the number of key tokens, and let $\mathbf{k}_{r, h}$ be the r -th key vector for attention head h . We define the average affinity between head h and \mathbf{K} as $a_h^{(j, \ell)}(\mathbf{K}) = \frac{1}{|\mathbf{K}|} \sum_{r=1}^{|\mathbf{K}|} \bar{\mathbf{q}}_h^{(j, \ell)\top} \mathbf{k}_{r, h}$. For each retrieved block e , we then measure the fraction of

attention heads whose affinity to the retrieved context exceeds that to the local window:

$$\rho_e^{(j,\ell)} = \frac{1}{H} \sum_{h=1}^H \mathbb{1} \left[a_h^{(j,\ell)}(\mathbf{K}_{\text{ret},e}^{(j,\ell)}) > a_h^{(j,\ell)}(\mathbf{K}_{\text{loc}}^{(j,\ell)}) \right]. \quad (8)$$

Since sink-collapse is associated with excessive inter-head attention homogenization, we retain the retrieved KV context only when all retrieved entries remain below a consensus threshold. Concretely, we define a binary gate $g^{(j,\ell)} = \mathbb{1}[\max_{1 \leq e \leq k} \rho_e^{(j,\ell)} \leq \tau_{\text{gate}}]$, where $\tau_{\text{gate}} \in (0, 1)$ is a consensus threshold. The resulting attention keys at block j , layer ℓ are then

$$\mathbf{K}_{\text{attn}}^{(j,\ell)} = \begin{cases} \text{Concat}_{\text{token}} \left(\mathbf{K}_{\text{ret},1}^{(j,\ell)}, \dots, \mathbf{K}_{\text{ret},k}^{(j,\ell)}, \mathbf{K}_{\text{loc}}^{(j,\ell)} \right), & g^{(j,\ell)} = 1, \\ \mathbf{K}_{\text{loc}}^{(j,\ell)}, & g^{(j,\ell)} = 0. \end{cases} \quad (9)$$

and the values $\mathbf{V}_{\text{attn}}^{(j,\ell)}$ are constructed analogously. This gating mechanism adds only a small number of dot-product operations per layer and does not alter the RoPE frequency spectrum or directly modify attention logits. It therefore preserves the original positional encoding structure while reducing collapse-prone attention patterns induced by retrieved context.

4.3 TRAINING DYSINK

DySink follows the two-stage streaming tuning paradigm of LongLive (Yang et al., 2025), which progressively transitions the model from short-horizon generation to long-horizon generation.

Stage 1: Short-horizon video distillation. We initialize from the Wan2.1-T2V-1.3B checkpoint (Wan et al., 2025) and perform Distribution Matching Distillation (DMD) (Yin et al., 2024) to obtain a few-step short-video generator (Huang et al., 2025; Yang et al., 2025). In this stage, a student denoiser (Wan2.1-T2V-1.3B) is distilled from a high-capacity teacher denoiser (Wan2.1-T2V-14B).

Stage 2: Long-horizon video fine-tuning. Starting from the distilled checkpoint, we fine-tune the generator on long streaming rollouts via LoRA (Hu et al., 2022; Chen et al., 2024; Yang et al., 2025). To ensure training-inference consistency, the complete DySink pipeline is enabled through training. In addition, we adopt two-segment prompt switching (Yang et al., 2025), where the conditioning prompt changes from p_1 to p_2 at a switching frame uniformly sampled from the valid rollout indices.

5 EXPERIMENTS

5.1 IMPLEMENTATION DETAILS

We build DySink on Wan2.1-T2V-1.3B (Wan et al., 2025), which generates 5-second clips at 16 FPS and 832×480 resolution. **Stage 1: Short-horizon video distillation.** We first adapt the pretrained model into a few-step causal-attention generator using a Self-Forcing DMD pipeline (Yin et al., 2024; Huang et al., 2025), trained on the extended VidProM prompts (Wang & Yang, 2024; Huang et al., 2025). This stage equips the model with short-window causal attention and the frame-sink mechanism (Yang et al., 2025), and is trained for 3,000 steps. **Stage 2: Long-horizon video fine-tuning.** We then fine-tune the Stage 1 model on 60-second sequences using LoRA, with Wan2.1-T2V-14B (Wan et al., 2025) as the teacher, following LongLive (Yang et al., 2025). We use PE-Core Encoder (Bolya et al., 2025) as the frozen visual encoder, and τ_{dedup} is set to 0.98. τ_{gate} is set to 0.5. Each training iteration extends the autoregressive rollout by one 5-second clip until reaching a maximum duration of 60 seconds. Meanwhile, a memory bank is maintained across blocks, and features from the local sliding-window blocks are aggregated to retrieve the top- k ($k=2$) relevant historical blocks, whose KV caches are injected to condition generation of the current block. We use a block size of 3 latent frames and a sliding window of 3 blocks. Stage 2 is also trained for 3,000 steps. **Optimization.** Following the DMD training setup, we optimize the generator (actor) and the distribution-matching critic using AdamW with $\beta_1 = 0.0$ and $\beta_2 = 0.999$. The learning rates are set to 1.0×10^{-5} for the actor and 2.0×10^{-6} for the critic. Training is conducted on 32 NVIDIA A100 GPUs with one sample per GPU, yielding a global batch size of 32. We further maintain an exponential moving average of the actor with decay 0.99, starting at step 200.

Table 1: Performance comparisons on 5s and 50s videos.

Model	#Params	Results on 5s \uparrow			Results on 50s \uparrow			
		Total Score	Quality Score	Semantic Score	Text Alignment	Temporal Quality	Dynamic Degree	Framework Quality
<i>Bidirectional models</i>								
LTX-Video	1.9B	80.00	82.30	70.79	-	-	-	-
Wan2.1	1.3B	84.67	85.69	80.60	-	-	-	-
<i>Autoregressive models</i>								
NOVA	0.6B	80.12	80.39	79.05	24.58	86.53	31.96	34.45
Pyramid Flow	2B	81.72	84.74	69.62	-	-	-	-
MAGI-1	4.5B	79.18	82.04	67.74	26.04	88.34	28.49	54.20
SkyReels-V2	1.3B	82.67	84.70	74.53	23.73	88.78	39.15	54.13
CausVid	1.3B	82.46	83.61	77.84	25.25	89.34	37.35	61.56
Self-Forcing	1.3B	83.00	83.71	80.14	24.77	88.17	34.35	61.06
Self-Forcing++	1.3B	83.11	83.79	80.37	26.37	91.03	55.36	60.82
LongLive	1.3B	83.10	83.57	81.23	28.08	89.29	42.40	65.75
DySink (Ours)	1.3B	83.92	84.68	80.87	28.39	91.63	63.52	64.87

Table 2: Performance comparisons on 75s and 100s long videos.

Model	Results on 75s \uparrow				Results on 100s \uparrow			
	Text Alignment	Temporal Quality	Dynamic Degree	Framework Quality	Text Alignment	Temporal Quality	Dynamic Degree	Framework Quality
<i>Autoregressive models</i>								
NOVA	23.37	86.32	31.24	31.53	22.89	86.24	31.09	31.03
MAGI-1	24.95	87.89	24.82	52.04	23.75	87.62	22.21	50.90
SkyReels-V2	22.70	88.99	39.89	51.55	22.05	88.80	38.75	50.48
CausVid	24.76	89.14	35.82	60.96	24.41	89.06	34.60	61.01
Self-Forcing	23.39	87.79	29.15	60.02	22.00	87.39	26.41	58.25
Self-Forcing++	26.31	91.00	55.62	60.67	26.04	90.87	54.12	60.66
LongLive	28.21	89.24	41.96	65.70	28.20	89.08	40.89	65.72
DySink (Ours)	28.40	91.62	62.75	64.89	28.36	91.39	60.72	64.68

5.2 EVALUATION

Evaluation Metrics We evaluate our model under two settings to assess both generation quality and temporal robustness. (1) **Short-horizon generation (5s)**: Following the VBench (Huang et al., 2024), we use 946 prompts across 16 dimensions, reporting the *Total Score*, *Quality Score*, and *Semantic Score* to quantify visual fidelity and semantic alignment. (2) **Long-horizon generation (50s, 75s, 100s)**: To examine the capacity for extended generation, we adopt a prompt set of 128 samples from MovieGen (Polyak et al., 2024), following the experimental setup of CausVid (Yin et al., 2025) and Self-Forcing++ (Cui et al., 2025). Performance in this setting is assessed with VBench Long, with evaluation focused on *Text Alignment*, *Temporal Quality*, *Dynamic Degree*, and *Framework Quality*. Together, these two settings provide a complementary evaluation of short-horizon generation quality and long-horizon temporal robustness.

Baseline methods We compare against several existing approaches, including NOVA (Deng et al., 2025), Pyramid Flow (Jin et al., 2024), SkyReels-V2-1.3B (Chen et al., 2025), MAGI-1-4.5B (Teng et al., 2025). We also include the similar autoregressive methods CausVid (Yin et al., 2025), Self-Forcing (Huang et al., 2025), Self-Forcing++ (Cui et al., 2025) and LongLive (Yang et al., 2025), all of which are 1.3B distilled few-step generators. For reference, two bidirectional models, LTX-Video (HaCohen et al., 2025) and Wan2.1-1.3B (Wan et al., 2025), are also evaluated.

Short-Horizon Generation (5s). As shown in Table 1, DySink achieves the highest Total Score among autoregressive methods, outperforming strong baselines such as Self-Forcing++ and LongLive while maintaining competitive Quality and Semantic scores. These results suggest that replacing static sinks with dynamic retrieval largely preserves short-horizon fidelity and semantic alignment.

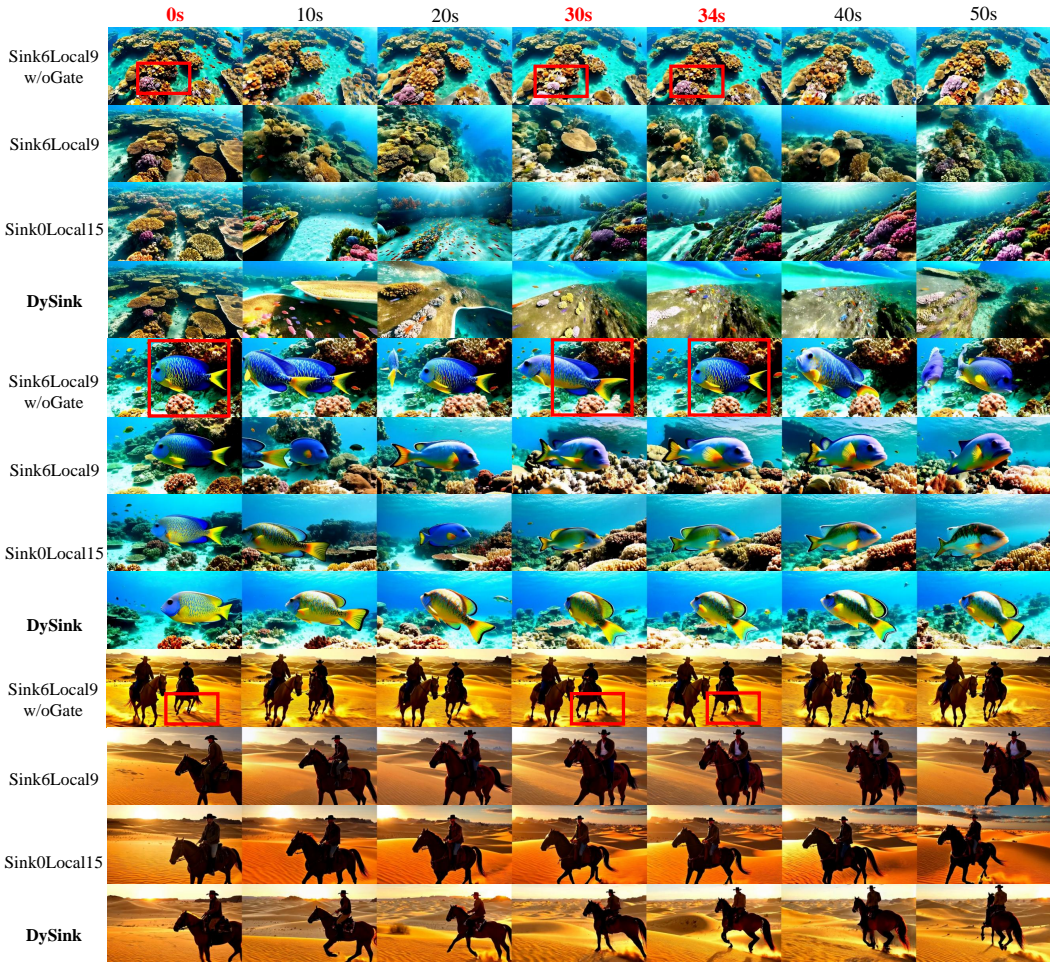


Figure 3: **Qualitative comparison of ablation variants on 50s video generation.** We show three representative long-horizon prompts covering underwater traversal, fish close-up, and desert horse-riding. Red boxes mark repeated structures caused by sink-collapse-like regression.

Long-Horizon Generation (50s / 75s / 100s). The advantages of DySink become more pronounced in long-horizon generation. Across the 50s, 75s, and 100s settings in Tables 1 and 2, DySink consistently achieves higher *Dynamic Degree* while maintaining strong measured *Temporal Quality*. Compared with Self-Forcing++, DySink improves *Dynamic Degree* by +8.16 / +7.13 / +6.60 points on 50s / 75s / 100s videos, respectively, with slightly higher *Temporal Quality*. These results indicate that the gains in *Dynamic Degree* are accompanied by strong measured *Temporal Quality*, consistent with our goal of supporting richer long-horizon evolution. Compared with LongLive, which relies on static sink frames for long-range stabilization, DySink achieves substantially higher *Dynamic Degree* (+21.12 / +20.79 / +19.83 on 50s / 75s / 100s videos), while also improving *Text Alignment* and *Temporal Quality*. We interpret the higher *Dynamic Degree*, together with the improved *Temporal Quality*, as evidence that DySink reduces temporal stagnation while preserving coherence, rather than merely increasing motion magnitude. Notably, this trend persists beyond the 60s training horizon: although DySink is fine-tuned on rollouts up to 60 seconds, it maintains high *Temporal Quality* and strong *Dynamic Degree* at both 75s and 100s.

5.3 ABLATION STUDY

We conduct ablation experiments on 50s video generation to analyze the effect of different long-range conditioning strategies. For a fair comparison, all variants are initialized from the same Stage-1

Table 3: Ablation Study on 50s videos. Bold highlights the highest, underline the second highest.

Metric	Sink6Local9-w/oGate	Sink6Local9	Sink0Local15	DySink
<i>Text Alignment</i> ↑	<u>28.33</u>	28.05	27.76	28.39
<i>Temporal Quality</i> ↑	88.98	<u>91.27</u>	90.90	91.63
<i>Dynamic Degree</i> ↑	37.98	<u>60.45</u>	57.27	63.52
<i>Framewise Quality</i> ↑	67.16	64.77	<u>64.88</u>	64.87

checkpoint and fine-tuned under the same training protocol, with an identical budget of 15 historical latent frames for the current generation. As shown in Table 3, we compare four variants: *Sink0Local15*, which uses only a local sliding window; *Sink6Local9*, which follows static-sink designs by combining 6 sink frames with a 9-frame local window; *Sink6Local9-w/oGate*, which removes the sink anomaly gate; and the full *DySink*, which uses dynamic retrieval together with the sink anomaly gate.

Comparing *Sink0Local15* and *Sink6Local9*, adding static sinks improves *Temporal Quality* from 90.90 to 91.27 and increases *Dynamic Degree* from 57.27 to 60.45. This suggests that, under this setting, fixed early-frame anchors can provide useful long-range cues beyond the local window. However, they remain less adaptive because the same early frames are reused regardless of the evolving visual state. In contrast, the full *DySink* further improves *Temporal Quality* to 91.63 and *Dynamic Degree* to 63.52, suggesting that visually retrieved historical context can preserve the stabilizing effect of long-range conditioning while better supporting long-horizon evolution.

The comparison between *Sink6Local9* and *Sink6Local9-w/oGate* highlights the role of the sink anomaly gate. Removing the gate decreases *Temporal Quality* from 91.27 to 88.98 and *Dynamic Degree* from 60.45 to 37.98, although it yields the highest *Framewise Quality*. This indicates that high per-frame quality alone can be misleading for long-horizon generation: visually plausible individual frames may still be accompanied by temporal stagnation or cyclic regression. Figure 3 provides qualitative evidence consistent with this interpretation. Without the gate, *Sink6Local9-w/oGate* tends to revisit earlier visual structures, including similar coral layouts in the underwater traversal, recurring fish poses and background patterns in the close-up fish scene, and repeated rider–horse configurations in the desert sequence. Adding the sink anomaly gate appears less prone to these sink-collapse-like repetitions, while *DySink* shows fewer repeated configurations and smoother long-horizon evolution.

6 CONCLUSION

In this work, we studied the limitations of static frame sinks for autoregressive long video generation, where fixed early-frame anchors can become mismatched with evolving visual states and may contribute to collapse-prone patterns. To address this issue, we proposed *DySink*, a retrieval-based alternative that maintains a compact memory bank and retrieves relevant context for long-range conditioning. *DySink* also incorporates a sink anomaly gate to detect excessive inter-head consensus and suppress the corresponding retrieved context. Experiments on minute-long video generation show that *DySink* consistently improves dynamic degree over strong methods while achieving higher temporal quality, demonstrating the benefit of dynamic frame sinks for long-horizon generation.

Limitations and Future Work. *DySink* has been evaluated on long-horizon generation up to 100 seconds, where many prompts involve smooth camera motion or gradual scene evolution. In such settings, the local window already provides strong short-term continuity, and the advantage of dynamic retrieval may not be fully exposed. We expect retrieval-based dynamic frame sinks to play a larger role in longer and more content-rich scenarios, such as object reappearance after long intervals, multi-stage scene transitions, or prompts with temporally structured events. In addition, *DySink* currently indexes memory using visual-only block descriptors. This lightweight design is partly motivated by the current stage of base video generators, which still struggle to reliably synthesize long videos with dense events, complex object interactions, and persistent narrative structure. As a result, more complex semantic understanding and retrieval mechanisms may be difficult to evaluate robustly under existing long-video generation settings. Nevertheless, visual-only descriptors may miss fine-grained temporal, object-level, or text-dependent cues. Future work may address this with stronger models and finer-grained understanding.

REFERENCES

- Daniel Bolya, Po-Yao Huang, Peize Sun, Jang Hyun Cho, Andrea Madotto, Chen Wei, Tengyu Ma, Jiale Zhi, Jathushan Rajasegaran, Hanoona Rasheed, Junke Wang, Marco Monteiro, Hu Xu, Shiyu Dong, Nikhila Ravi, Daniel Li, Piotr Dollár, and Christoph Feichtenhofer. Perception encoder: The best visual embeddings are not at the output of the network. *arXiv preprint arXiv:2504.13181*, 2025.
- Guibin Chen, Dixuan Lin, Jiangping Yang, Chunze Lin, Junchen Zhu, Mingyuan Fan, Hao Zhang, Sheng Chen, Zheng Chen, Chengcheng Ma, et al. Skyreels-v2: Infinite-length film generative model. *arXiv preprint arXiv:2504.13074*, 2025.
- Yukang Chen, Shengju Qian, Haotian Tang, Xin Lai, Zhijian Liu, Song Han, and Jiaya Jia. Longlora: Efficient fine-tuning of long-context large language models. In *ICLR*, 2024.
- Justin Cui, Jie Wu, Ming Li, Tao Yang, Xiaojie Li, Rui Wang, Andrew Bai, Yuanhao Ban, and Cho-Jui Hsieh. Self-forcing++: Towards minute-scale high-quality video generation. *arXiv preprint arXiv:2510.02283*, 2025.
- Justin Cui, Jie Wu, Ming Li, Tao Yang, Xiaojie Li, Rui Wang, Andrew Bai, Yuanhao Ban, and Cho-Jui Hsieh. Lol: Longer than longer, scaling video generation to hour. *arXiv preprint arXiv:2601.16914*, 2026.
- Haoge Deng, Ting Pan, Haiwen Diao, Zhengxiong Luo, Yufeng Cui, Huchuan Lu, Shiguang Shan, Yonggang Qi, and Xinlong Wang. Autoregressive video generation without vector quantization. In *ICLR*, 2025.
- Patrick Esser, Sumith Kulal, Andreas Blattmann, Rahim Entezari, Jonas Müller, Harry Saini, Yam Levi, Dominik Lorenz, Axel Sauer, Frederic Boesel, et al. Scaling rectified flow transformers for high-resolution image synthesis. In *Forty-first international conference on machine learning*, 2024.
- Yuwei Guo, Ceyuan Yang, Hao He, Yang Zhao, Meng Wei, Zhenheng Yang, Weilin Huang, and Dahua Lin. End-to-end training for autoregressive video diffusion via self-resampling. *arXiv preprint arXiv:2512.15702*, 2025.
- Yoav HaCohen, Nisan Chiprut, Benny Brazowski, Daniel Shalem, Dudu Moshe, Eitan Richardson, Eran Levin, Guy Shiran, Nir Zabari, Ori Gordon, et al. Ltx-video: Realtime video latent diffusion, 2025. *arXiv preprint arXiv:2501.00103*.
- Edward J Hu, Yelong Shen, Phillip Wallis, Zeyuan Allen-Zhu, Yuanzhi Li, Shean Wang, Lu Wang, and Weizhu Chen. LoRA: Low-rank adaptation of large language models. In *ICLR*, 2022.
- Xun Huang, Zhengqi Li, Guande He, Mingyuan Zhou, and Eli Shechtman. Self forcing: Bridging the train-test gap in autoregressive video diffusion. *arXiv preprint arXiv:2506.08009*, 2025.
- Ziqi Huang, Yinan He, Jiashuo Yu, Fan Zhang, Chenyang Si, Yuming Jiang, Yuanhan Zhang, Tianxing Wu, Qingyang Jin, Nattapol Chanpaisit, et al. Vbench: Comprehensive benchmark suite for video generative models. In *Proceedings of the IEEE/CVF Conference on Computer Vision and Pattern Recognition*, pp. 21807–21818, 2024.
- Sihui Ji, Xi Chen, Shuai Yang, Xin Tao, Pengfei Wan, and Hengshuang Zhao. Memflow: Flowing adaptive memory for consistent and efficient long video narratives. *arXiv preprint arXiv:2512.14699*, 2025.
- Yang Jin, Zhicheng Sun, Ningyuan Li, Kun Xu, Hao Jiang, Nan Zhuang, Quzhe Huang, Yang Song, Yadong Mu, and Zhouchen Lin. Pyramidal flow matching for efficient video generative modeling. *arXiv preprint arXiv:2410.05954*, 2024.
- Yaron Lipman, Ricky TQ Chen, Heli Ben-Hamu, Maximilian Nickel, and Matt Le. Flow matching for generative modeling. *arXiv preprint arXiv:2210.02747*, 2022.
- Kunhao Liu, Wenbo Hu, Jiale Xu, Ying Shan, and Shijian Lu. Rolling forcing: Autoregressive long video diffusion in real time, 2025. *arXiv preprint arXiv:2509.25161*.

- Yunhong Lu, Yanhong Zeng, Haobo Li, Hao Ouyang, Qiuyu Wang, Ka Leong Cheng, Jiapeng Zhu, Hengyuan Cao, Zhipeng Zhang, Xing Zhu, et al. Reward forcing: Efficient streaming video generation with rewarded distribution matching distillation. *arXiv preprint arXiv:2512.04678*, 2025.
- OpenAI. Video generation models as world simulators. Technical report, 2024.
- William Peebles and Saining Xie. Scalable diffusion models with transformers. In *ICCV*, pp. 4172–4182, 2023.
- Adam Polyak, Amit Zohar, Andrew Brown, Andros Tjandra, Animesh Sinha, Ann Lee, Apoorv Vyas, Bowen Shi, Chih-Yao Ma, Ching-Yao Chuang, et al. Movie gen: A cast of media foundation models. *arXiv preprint arXiv:2410.13720*, 2024.
- Team Seedance, De Chen, Liyang Chen, Xin Chen, Ying Chen, Zhuo Chen, Zhuowei Chen, Feng Cheng, Tianheng Cheng, Yufeng Cheng, et al. Seedance 2.0: Advancing video generation for world complexity. *arXiv preprint arXiv:2604.14148*, 2026.
- Jianlin Su, Murtadha Ahmed, Yu Lu, Shengfeng Pan, Wen Bo, and Yunfeng Liu. Roformer: Enhanced transformer with rotary position embedding. *Neurocomputing*, 568:127063, 2024.
- Hansi Teng, Hongyu Jia, Lei Sun, Lingzhi Li, Maolin Li, Mingqiu Tang, Shuai Han, Tianning Zhang, WQ Zhang, Weifeng Luo, et al. Magi-1: Autoregressive video generation at scale. *arXiv preprint arXiv:2505.13211*, 2025.
- Team Wan, Ang Wang, Baole Ai, Bin Wen, Chaojie Mao, Chen-Wei Xie, Di Chen, Feiwu Yu, Haiming Zhao, Jianxiao Yang, et al. Wan: Open and advanced large-scale video generative models. *arXiv preprint arXiv:2503.20314*, 2025.
- Wenhao Wang and Yi Yang. Vidprom: A million-scale real prompt-gallery dataset for text-to-video diffusion models. *Advances in Neural Information Processing Systems*, 37:65618–65642, 2024.
- Guangxuan Xiao, Yuandong Tian, Beidi Chen, Song Han, and Mike Lewis. Efficient streaming language models with attention sinks. *arXiv preprint arXiv:2309.17453*, 2023.
- Shuai Yang, Wei Huang, Ruihang Chu, Yicheng Xiao, Yuyang Zhao, Xianbang Wang, Muyang Li, Enze Xie, Yingcong Chen, Yao Lu, et al. Longlive: Real-time interactive long video generation. *arXiv preprint arXiv:2509.22622*, 2025.
- Yang Yang, Tianyi Zhang, Wei Huang, Jinwei Chen, Boxi Wu, Xiaofei He, Deng Cai, Bo Li, and Peng-Tao Jiang. Anchor forcing: Anchor memory and tri-region rope for interactive streaming video diffusion. *arXiv preprint arXiv:2603.13405*, 2026a.
- Ying Yang, Zhengyao Lv, Tianlin Pan, Haofan Wang, Binxin Yang, Hubery Yin, Chen Li, Ziwei Liu, and Chenyang Si. Stableworld: Towards stable and consistent long interactive video generation. *arXiv preprint arXiv:2601.15281*, 2026b.
- Jung Yi, Wooseok Jang, Paul Hyunbin Cho, Jisu Nam, Heeji Yoon, and Seungryong Kim. Deep forcing: Training-free long video generation with deep sink and participative compression. *arXiv preprint arXiv:2512.05081*, 2025.
- Tianwei Yin, Michaël Gharbi, Richard Zhang, Eli Shechtman, Frédo Durand, William T Freeman, and Taesung Park. One-step diffusion with distribution matching distillation. In *CVPR*, 2024.
- Tianwei Yin, Qiang Zhang, Richard Zhang, William T Freeman, Fredo Durand, Eli Shechtman, and Xun Huang. From slow bidirectional to fast autoregressive video diffusion models. In *CVPR*, 2025.
- Jiwen Yu, Jianhong Bai, Yiran Qin, Quande Liu, Xintao Wang, Pengfei Wan, Di Zhang, and Xihui Liu. Context as memory: Scene-consistent interactive long video generation with memory retrieval. In *Proceedings of the SIGGRAPH Asia 2025 Conference Papers*, pp. 1–11, 2025a.
- Yifei Yu, Xiaoshan Wu, Xinting Hu, Tao Hu, Yangtian Sun, Xiaoyang Lyu, Bo Wang, Lin Ma, Yuewen Ma, Zhongrui Wang, and Xiaojuan Qi. Videossm: Autoregressive long video generation with hybrid state-space memory. *arXiv preprint arXiv:2512.04519*, 2025b.

Shenghai Yuan, Yuanyang Yin, Zongjian Li, Xinwei Huang, Xiao Yang, and Li Yuan. Helios: Real real-time long video generation model. *arXiv preprint arXiv:2603.04379*, 2026.

Lvmin Zhang, Shengqu Cai, Muyang Li, Chong Zeng, Beijia Lu, Anyi Rao, Song Han, Gordon Wetzstein, and Maneesh Agrawala. Pretraining frame preservation in autoregressive video memory compression. *arXiv preprint arXiv:2512.23851*, 2025.

Zengqun Zhao, Yanzuo Lu, Ziquan Liu, Jifei Song, Jiankang Deng, and Ioannis Patras. Relax forcing: Relaxed kv-memory for consistent long video generation. *arXiv preprint arXiv:2603.21366*, 2026.

Hongzhou Zhu, Min Zhao, Guande He, Hang Su, Chongxuan Li, and Jun Zhu. Causal forcing: Autoregressive diffusion distillation done right for high-quality real-time interactive video generation. *arXiv preprint arXiv:2602.02214*, 2026.